2008 IEEE International Conference on
Robotics and Automation
Pasadena, CA, USA, May 19-23, 2008

Simulation And Experimental Evaluation Of Laser-Structured Actuators For A Mobile Microrobot

C. Edeler

Abstract— **This paper describes the simulation, fabrication and evaluation of a mobile platform's actuator, which is the foundation for microrobots. The working principle is based on the mobile platform RollBot. The new feature is the combination of three rolling steel spheres driven by three laser structured piezoactuators, each containing three ruby hemispheres. Because of the piezoactuator's special design, the hemisphere's stick-slip displacements decrease and enable a more precise control. The platform's properties concerning rigidity, resolution and maximum velocity improve. After an introduction of RollBot's and the new actuation principle, a short description of the laser structuring process is given. Several Finite-Element(FE)-simulations are presented to understand the expected performance of the mobile platform. Finally, measurements of step sizes and maximum velocities are shown. The application of the actuator in a mobile platform proves the derived properties.**

I. Introduction

The importance of reliable positioning devices in the microsystem technology is unchallenged. The requirements for precise and rugged robotic devices are still increasing. Higher accuracy, quicker movement and more robust handling are demanded [1], [2]. Many systems are built on microrobots to meet the given needs. Martel *et al.* presented the Nanowalker system [3], [4]. Piezotubes can bend and elongate, thus a stick-slip motion can be established. Driesen *et al.* use flexure hinges and bending piezo elements to drive their mobile platforms [5], [6]. Aoyama presented microrobots using piezoelements and magnetic coils for their drive [7], [8]. All systems have in common, that they use mobile microrobots with piezoactuators to perform motion. All mobile microrobots feature a large working space typically only limited by wires. A possibility to meet the requirements of mobile microrobots was proceeded by the Division Microrobotics and Control Engineering in recent years. The system described in this paper is based on these mobile microrobots. As described in [9] mobile robotic systems can be generally subdivided into three parts:

- An endeffector to perform the desired handling task. Endeffectors can be: needles, tips or grippers.
- A manipulator for the positioning of the endeffector. The manipulator provides all essential degrees of freedom for operating tasks.
- A mobile platform to transport the manipulator and the endeffector to the working area and assist at handling operations. An in-plane mobile platform offers two translational degrees of freedom (x and y) and one rotational degree of freedom (Φ). The degrees of freedom of the manipulator and the mobile platform complement one another in the ideal case.

Advantages linked to this approach are the relatively high working distances in combination with high accuracy and the availability of satisfactory degrees of freedom. Because the actuation principle is based on common acoustic piezodiscs, some drawbacks like low rigidity and susceptibility for parasitic vibrations were detected [10]. The new actuator concept replaces the elastic piezodiscs with optimized laser-cut piezoactuators, leading to much higher resonance frequencies and less load-dependent behavior.

II. RollBot's and new working principle

A. Working principle of RollBot

The previous working principle relies on a segmented piezodisc and three rotating steel spheres [11], [12], [13]. The steel spheres carry the platform itself and roll up on the working surface. Each steel sphere is driven by three smaller ruby spheres, which are attached to several segments of the piezodisc. As illustrated in Fig. 1, bending of a piezodisc segment leads to a displacement of the ruby sphere, which drives the steel sphere. Fig. 1a shows the static state. In Fig. 1b the piezosegment bends slowly, which leads to a rotation of the steel sphere (stick phase). After a quick bending upwards the steel sphere did not move, Fig. 1c (slip phase). When the bending segment has returned into the static state (Fig. 1d), the steel sphere turned a slightly bit and one stick-slip-step is completed. The step size of RollBot is 110 nm, the maximum velocity about 1.5 mm/s. The major

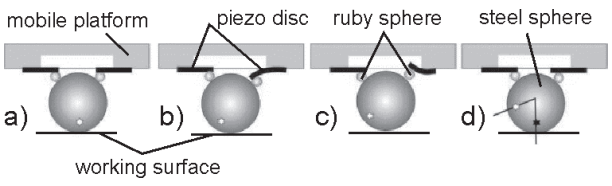

Fig. 1. Schematic illustration of the previous actuation principle. A common piezodisc bends and drives one of three steel sphere's, the mobile platform moves (step a-d)

Manuscript received September 4, 2007. Christoph Edeler is with the Division Microrobotics and Control Engineering, University of Oldenburg, 26111 Oldenburg, Germany. He studied mechanical engineering at the university RWTH-Aachen, Germany, with the major field construction and development. He completed his degree with an external diploma thesis in the company CLAAS harvesting machines, Harsewinkel, Germany, finishing in March 2006. Now he works in the Department Microrobotics and Control Engineering since June 2006. Projects: NanoHand EU, ZuNaMi (BMBF), RoboMat (BMBF), Nanostore (BMBF). (phone: +049-441-798-4296; fax: +049-441-798-4267; E-mail: christoph.edeler@kisum.uni-oldenburg.de)

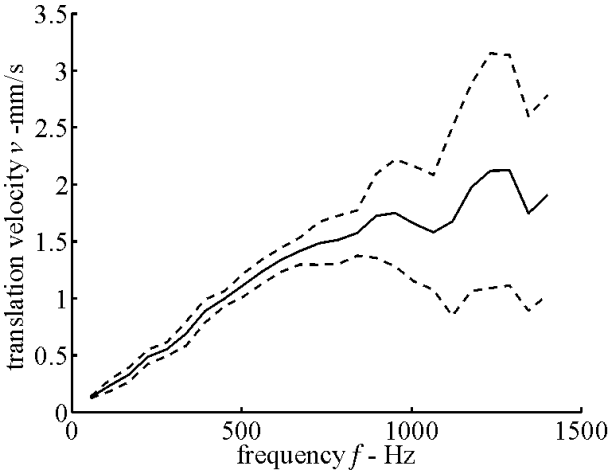

Fig. 2. Dependency of the RollBot platform's translation velocity against control frequency (solid line). Above 750 Hz the velocity's variance increases (dashed lines) [10]

advantage of this principle is, that the "slip" of the stick-slip takes place between the ruby and the steel sphere. In older versions the stick-slip contact occured directly between the mobile platform and the working surface. This resulted in increased wear of the working surface and led to further positioning problems. Due to the "indirect" working principle the requirements for the working surface are much lower. This idea is kept in the new approach. Additionally, the RollBot is built of cheap parts and comparatively easy to manufacture. A major disadvantage can be seen in the non-rigid properties of the piezodisc. Fig. 2 shows that a sawtooth control frequency above 750 Hz does not lead to an increased velocity, but to a dramatic increase of the variance (dashed lines). In fact, the system behaviour becomes chaotic, no controlled motion is possible. This is an indicator for the low eigenfrequencies of the system. The piezodisc works as a bending actuator, which produces low forces in combination with relatively high displacements. Furthermore, the masses of the ruby spheres (Fig. 1) must be accelerated, which decreases performance. A course analysis of the first piezodisc's eigenmode leads to a frequency of 1.35 kHz.

B. New working principle with lasercut piezoactuators

The new approach makes use of the inverse piezoelectric effect of a solid PZT ceramic plate to drive the ruby hemispheres directly. The piezoceramic plate has dimensions of 10x10 mm^2 and a thickness of 500 μm. The two larger surfaces are delivered with an electrically conductive coating as electrodes. The ceramic's properties are shown in Table I. The vector of the piezoelectric charge constant d_{33} runs perpendicular to the electrode surfaces. The bottom electrode is assumed to be connected to ground (Fig. 3b, c). The upper electrode is subdivided into several functional structures, which are not connected to each other electrically (Fig. 3a). The piezoceramic incorporates four contact pads for each of the ruby hemisphere's, which leads to twelve contact pads plus circuit paths and solder pads. Three ruby hemispheres with a diameter of 1 mm are attached to the structured pads with adhesive (Fig. 3b). The piezoceramic is controlled in such a way, that the ruby hemispheres can be rotated by a displacement of the piezoceramic surfaces. The displacement is generated by applying symmetric potentials to pads lying opposite to each other. When symmetric voltages are applied to the electrodes as in Fig. 3c, the upper surfaces of the ceramic move down and up as the arrows indicate. This results in a rotation of the ruby hemisphere around a point close to its centre. The motion is assigned to the steel sphere, if an adequately slow motion is used (stick phase). Thus, control using symmetric voltages leads to a rotation of the rolling up steel sphere. As the mobile platform is supported by three steel spheres with actuators, the mobile platform moves into a defined direction.

The new design combines the beneficial stick-slip contact point not lying on the working surface with the advantages of rigid piezoceramics. Fig. 4 shows a Computer Aided Design (CAD) actuator model (left), and a functional model (right). The fabrication of the laser-structured pads and the whole actuator is described in part III. As shown in Fig. 4, the steel

TABLE I
DATA OF PIEZOCERAMIC

Material:	PZT-5H
Charge constants	
d_{33}	500*10^{-12}C/N
d_{31}	-210*10^{-12}C/N
Elastic compliance	
S_{33}	19*10^{-12}m²/N
Curie temperature	250°C
Poisson's ratio	0.34
Static compressive strength	>600MPa

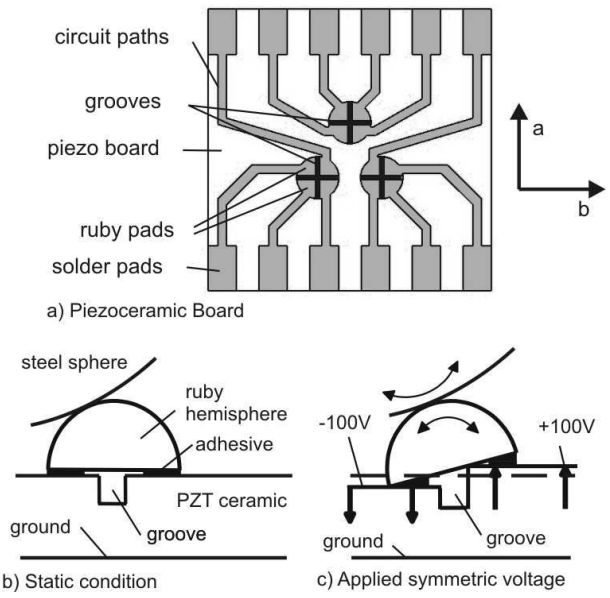

Fig. 3. Working principle of the piezoactuator: a) the piezoceramic structure, b) the actuator in its static condition, c) the actuator is applied with symmetric voltage, the ruby hemisphere turns and drives the steel sphere

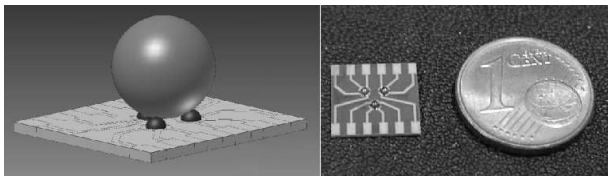

Fig. 4. Piezoceramic actuator. Left: Computer Aided Design (CAD), Right: Functional model without steel sphere

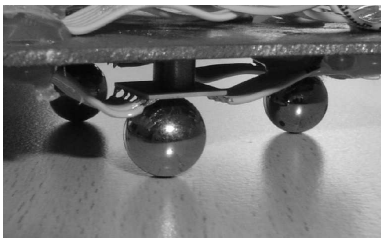

Fig. 5. Photo of the mobile platform prototype

sphere lies on three ruby hemispheres. Analogously to the previous working principle, the combination of three steel sphere motions defines the degrees of freedom of the mobile platform. If all steel sphere rotation axes are parallel to each other, the platform moves straight forward. If the axes have an intersection point, the platform rotates around that point.

Due to the low displacements of a piezoceramic even at high voltages, the attained displacements are very small. The piezoceramic is made of a typical mechanically "soft" ceramic, it consists of lead zirconate - lead titanate (PZT). Equation (1) shows the fundamental relation between Voltage, charge constant and displacement:

$$d_L = d_{33} \cdot n \cdot U. \tag{1}$$

As the actuator consists of a single layer with a thickness of 500 μm, n equals 1. Also for a typical control voltage of $\pm$100 V (U) and piezo data from Table I (d_{33}) the displacement d_L equals 50 nm. That means, the theoretical static displacement of one surface or the hemisphere's tip for the rotational case, respectively, can generate a motion of the mobile platform of 50 nm. This is a weak value in terms of an achieveable maximum velocity, but in terms of accuracy, an average gradient of 0.5 nm/V is promising.

The stiffness of the ceramic in Table I is denoted as 600 MPa, but this is a theoretical value due to the refractory properties of ceramics. A more realistic stiffness is represented by the elastic compliance. It is the reciprocal value of the raw piezoceramic stiffness, which can be calculated to be 52 GPa. This is by far a higher stiffness then the older bending actuator could offer. However, the influence of mechanical and electrical conditions is great, and it is nearly impossible to measure or compute the real rigidity of the piezoceramic, especially when it is structured like in Fig. 3a. Nevertheless, the piezoactuator is advantageous in terms of mechanical properties.

At least the verification of the mechanical solidness of the piezoceramic actuator is done. As the vendor of the ceramics (PI, Germany) states, the maximum pressure in operation must not exceed 20 % of 250 MPa. If the mobile platform weights about 80 g and it lies on nine ruby hemispheres with a diameter of 1 mm, the pressure in static condition is about 100 kPa. Valuation of the dynamic stress is very difficult, but even if the local dynamic actuation pressure is estimated to be 100 times higher due to the rapid stick-slip-acceleration, the actuator can be considered as fully operational.

The combination of the driving technique described above with stick-slip principle aims at an almost continuous rotation of the steel sphere. Brought forward to the mobile platform, an infinite motion in every degree of freedom should be possible. Advantages of this working principle are:

- The actuator has an increased rigidity because of the use of raw piezoceramic instead of a disc with bending elements. This leads to less vibrations and increased eigenfrequencies.
- The distribution of forces through the actuator is more direct. The resonance frequencies rise because the major obstructive element, the bending disc, is left out.
- The accuracy rises because a higher voltage leads to a lower displacement.

Additionally, permanent magnets are used to improve the stick-slip performance. One magnet per steel sphere is mounted on the ground side of the piezoceramics. With its attraction force it pulls the steel sphere onto the ruby hemispheres. This increases friction at the stick-slip contact points, without rising the overall mobile platforms weight and inertia critically. There is no influence of the magnets on the piezoceramic actuator, because the actuators use an electric field. Nevertheless, further shielding will be necessary when using the permanent magnets in a Scanning Electron Microscope (SEM). Fig. 5 shows a photo of the new actuator in the mobile platform.

III. Laser structuring process

A low power Nd-YAG laser milling device (LaserplussAG, Germany) with X-Y-table and Z-axis is used to structure the piezoceramic plates. With a maximal power of 8 W the focus point has a diameter of less than 10 μm [14]. The plates are delivered with an electroconductive coating, which serves as actuator electrode. The laser structuring process, based on sequential linescans, allows both conditioning of the coating (Segmentation), and removing material in depth (Structuring). First of all, the electrode geometry is segmented, as shown in Fig. 3a. Grey patterns represent electroconductive structures, white patterns stand for removed coating. After this process step, pads for the ruby hemispheres, twelve solder pads at the edges and circuit paths are available. In a second step, grooves are fabricated between the hemisphere pads in the piezoceramic (Fig. 3a, black crosses). The grooves enable a free movement of the pads and avoid destructive high stress under the rotating ruby hemispheres. The fabrication of both actuator and electrode geometry in two consecutive steps is very advantageous. This approach comprises potential for further miniaturization

and variations of the concept. Because the laser process works with low power and short pulse times about 30 ns the thermal influence on unstructured PZT material is negligible. So the ceramic material near to structured edges is not affected or depolarized, even with the low curie temperature of the ceramic of 250 °C. This is important because a "re"-polarization voltage of 1 kV would induce short circuits and breaks in the circuit paths.

IV. Simulation

To investigate the performance of the designed actuators, Finite-Element (FE) simulations with Comsol Multiphysics based on the CAD-model (Fig. 4, left) were done. In a first step, the estimated displacement in z-direction (thickness direction) of the raw actuator was determined. Only one pad set was modeled to limit the model's solution times. Fig. 6 shows a contact-pad set for one of the three ruby hemispheres. The outer pair of solder pads was modeled with 100 V, the inner pair with -100 V. The blind surface on the lower side is modeled with ground potential (zero voltage). It represents the general backing electrode of the actuator. 100 V in any polarity is nonhazardous due to 1 kV polarization limit.

The simulation shows a positive z-displacement for the surfaces with positive potential (Fig. 6, coloured black) of 58 nm. Analogously, the displacement of the -100 V electrodes (Fig. 6, coloured white) is -57 nm. The grey surfaces in between represent a displacement of zero. The positive and negative displacements are as they were expected, a value of 50 nm was derived from theory.

When the displacement in z was observed, a "parasitic motion" induced by the z-displacement was observed. As Table I shows, the ceramic material's Poisson's ratio is about one third. So, a deformation in x or y is unavoidable. Exemplarily, Fig. 7 shows the same FE-model as in Fig. 6, but with y-displacement coloured. The average displacement is less then 10 nm. But there are some maxima near to material edges about 50 nm, particularly close to the solder pads and the groove between the hemisphere pads. The maxima arise from the continuous ground electrode. Thereby the density of the electrical streamlines increases towards structured electrode edges.

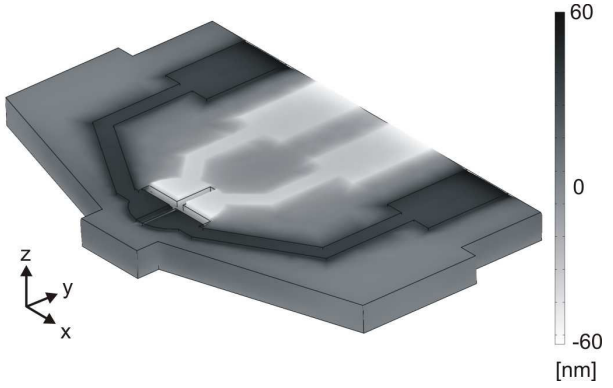

Fig. 6. Z-displacement of the pads for a rotation of the ruby hemisphere

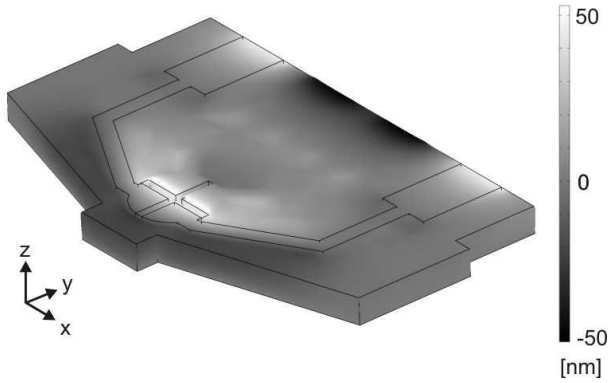

Fig. 7. Y-displacement of the ceramic plate

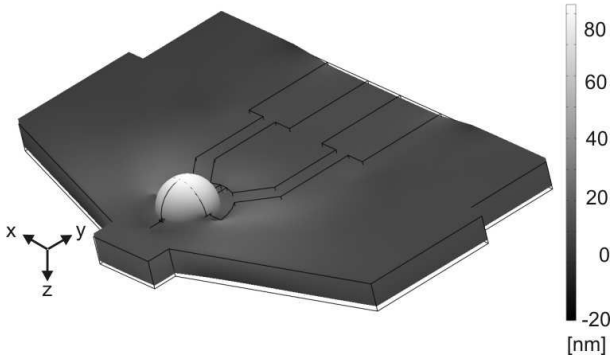

Fig. 8. Y-displacement of the ruby hemisphere's tip

Due to this coherency, the displacements in z and y increase. Generally, the parasitic motion is less distinctive than the motion in z-direction, and any motion close to the solder pads can be neglected. Nevertheless, the parasitic motion at the hemisphere pads needs to be considered carefully. It is conceivable that the maxima have a bad influence on the hemisphere's motion. This could lead to a displacement of the joints between ruby hemisphere and piezoceramic and further to a different displacement ratio or a changed attitude of the motion axes. For the discussion it is assumed that the adhesive levels the maxima under the ruby hemispheres and therefore causes no disturbing influence.

The ruby hemisphere's tip displacement is shown in Fig. 8. This simulation must be done in a separate FE-model because of technical reasons [15]. White surfaces mark displacements in y-direction. The displacements of the actuator including a 30 μm thick adhesive are shown. Due to technical reasons the coordinate system turned. Thus, the voltages are modeled inversely to Fig. 6. The hemisphere's tip moves into the estimated direction. The "highest" point of the hemisphere moves 95 nm in y-direction. This is twice as much as expected, because the estimated displacement is about 50 nm due to geometric reasons. Possibly the edge maxima identified in Fig. 7 are the reason for this discrepancy and displace the geometrical joint points between ceramic and ruby. Secondly, a bending effect of the whole ceramic is identified. But this bending displacement is less than 20 nm at the outer borders and can be ignored. Finally,

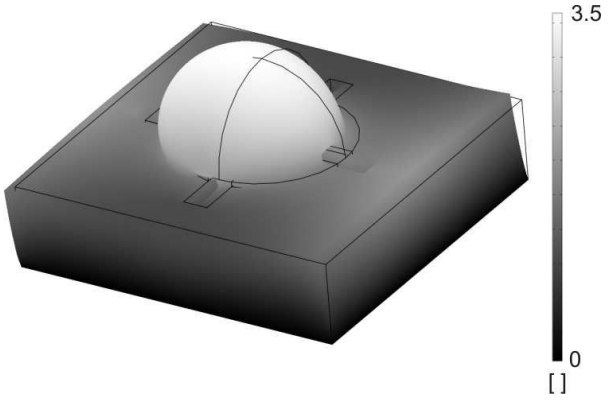

Fig. 9. Critical eigenmode at 975 kHz: the ruby hemisphere rotates in the same manner as in the actuator (Fig. 3)

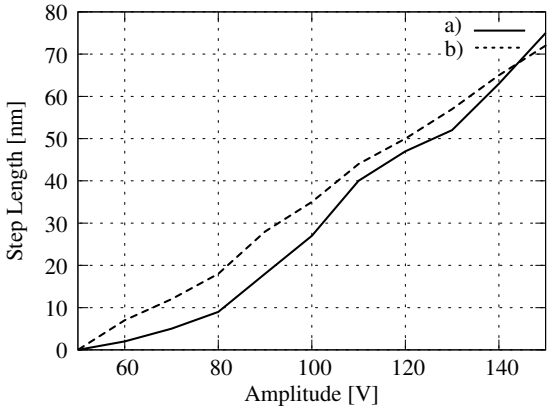

Fig. 10. Step length over control voltage (single experiment) of a) the main axis, b) the secondary axis

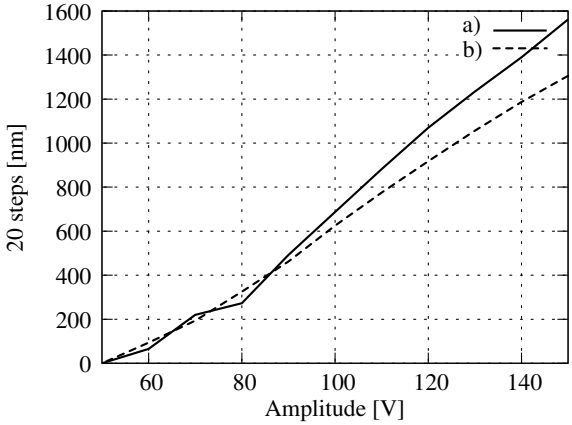

Fig. 11. Length of 20 steps over control voltage (single experiment) of a) the main axis, b) secondary axis

the upper bound for possible control frequencies shall be determined. Although there are many unknown properties such as dynamical aspects, electric control properties or exact mechanical loads and forces, an estimation can be done. This is possible because of the fact that the material stiffness and the inertia can be estimated or simulated, respectively, and these values have most of the influence on the critical eigenfrequency. As the elastic compliance S_{33} indicates, the stiffness is practically about 52 GN/m^2. But this is only a coarse assessment. Fig. 9 shows a characteristic eigenmode, which could be critical for the function of the actuator's. The FE-model contains a single hemisphere, adhesive and partly the piezoceramic plate. The ruby hemisphere moves in the same way as the actuator drives it normally. The eigenfrequency of this eigenmode is a very high value with 975 kHz. One reason is, that the stiffness of the structured plate is very high and the mass of the hemisphere very low. As a final remark it can be said that critical eigenfrequencies are located in the range of some hundred kilohertz and should not be a problem for typical control frequencies in the range up to maximal 50 kHz. From this point of view the actuator's high stiffness allows very high control frequencies.

V. Results

A. Experiments

The experiments to determine the platforms accuracy were done with the laser interferometer SIOS SP-S 120. Two light-reflecting pieces of silica are mounted on the mobile platform, perpendicular to each other. These mirrors are adjusted to the estimated motion directions. One direction is defined as the a-direction in Fig. 3a, i.e. the steel sphere rotates towards this direction, it is further named the main axis. The direction perpendicular to 'a' is called 'b', the secondary axis. The required voltages were generated using a switching amplifier, which supports high slew rates in combination with high amplitudes. Rotational movements could not be measured. To get an overview about the platform's ability to perform stick-slip steps, the achieved step lengths in both axes over different amplitudes are shown in Fig. 10. An amplitude voltage in Fig. 10 (e.g. 80 V) means, the electrodes are driven with $\pm$80 V, *i.e.* to get the according step value for symmetric voltages, the step size must be multiplied by two. Amplitude voltages between 50 and 150 V are presented, because amplitudes below 50 V do not cause any measurable motion. From 50 to 150 V a coarsely linear relation can be determined. The smallest steps which can be achieved are less than 10 nm at 60 V. The simulated case of $\pm$100 V corresponds to an amplitude of 200 V, which could not be measured due to technical reasons. Extrapolating to 200 V, a step size of 100 nm can be assumed. There are small differences in the step sizes between the main and secondary axis in the range of few nanometers, but in general the same linear behavior can be identified.

To investigate the influence of dynamic aspects, the same measurement is done, but having a look at the complete distance performed by 20 steps. The steps are generated with a frequency of 8 kHz. Fig. 11 shows the result. Accordingly to the single steps, amplitudes below 50 V have no effect. Between 50 and 150 V the covered distance grows linearly from zero to 1550 nm for the main axis (Fig. 11a) and to 1300 nm for the secondary axis (Fig. 11b). Assuming equal step sizes, the re-calculated single step sizes are similar to the measured single step lengths from Fig. 10. The deviation

is less than 10%, so the influence of dynamical aspects is practically not existent even at comparatively high control frequencies.

The platform's properties concerning the ability to rotate could not be measured. Because only one laser-interferometer is available and the exact position of the geometrical rotation point is unknown, it is difficult to design an adequate measurement setup.

To determine the maximum platform's velocity a further experiment was done. With a symmetrical voltage of $\pm 100\,\mathrm{V}$ and a control frequency of 18 kHz a velocity of 1.5 mm/s was achieved. Compared to the RollBot's performance (Fig. 2), the new design's variance is much lower ($<5\%$) and linear up to 18 kHz.

B. Discussion

In part II the displacement of the ruby hemisphere's tip with 100 V was derived from theory to be 50 nm. This means a single step length of 100 nm, because the stick-slip phase uses displacements in both directions. As the simulation in part IV describes, the tip's displacement is about 60 nm which leads to a step size of 120 nm. This is a good accordance to the theory. Both theory and simulation use a linear approach, so the displacements can be interpolated down to zero. Finally, the measurements yield a step size of about 120 nm under the same voltage conditions. For this working point, theory and practice are correlated very well. A discrepancy is the fact, that amplitudes under 50 V do not cause a measurable effect. As this effect does not occur in static measurements, it is likely that no slip phase can be established. This happens because the displacements are too low or the inertia of the platform is too small to overcome static friction. Nevertheless, single steps with an accuracy of 10 nm are possible, this is ten times less than the RollBot platform can do.

Static voltages can be used to move the platform with very high accuracy. Under this condition the accessible resolution is in the range of a single nanometer, because $\pm 50\,\mathrm{V}$ induce 30 nm displacement. That is approximately a rate of 0.5 nm/V. The simulation of critical eigenmodes and preliminary results indicate, that control up to 50 kHz are possible. In combination with high amplitudes a maximum velocity of about 6 mm/s at 18 kHz was measured, which is four times higher than the RollBot's performance. The theoretical limitation for the control frequencies is reached, when the stick phase is too short for the spheres to follow due to their inertia. However, because of many unknown influences like dynamic friction coefficients, it can not be calculated.

VI. Conclusion and Outlook

As the results are very promising, further improvements of the concept are planned. First of all, miniaturization can be done. A concept including all nine ruby hemispheres on a single piezoceramic plate is thinkable. However, the electrical connection to the voltage amplifiers, specially the wiring is a problem for manufacturing and handling. The piezoceramic plates are mechanically delicate and improper soldering of wires can damage the conductive adhesive. Another problem is the wiring of the 36 electrodes. Both problems could be eliminated using a circuit board, which is mechanically adapted to alleviate soldering without using wires and electrically adapted to combine channels with equal potentials. In theory, the miniaturization is only limited by the size of the spheres and finally by the precision of the laser structuring process. A robot-based manufacturing could help to position smaller ruby hemispheres.

As the actuator is able to drive a steel sphere in any direction and also works upside down, it could be used as a multi degree of freedom specimen holder for applications under a light microscope or in an SEM. Using the bottom half of a sphere and placing the specimen in the sphere's centre, an eucentric micromanipulator is thinkable.

Acknowlegement

This work was supported by the European Commission, FP6 Integrated Project NanoHand, IST-5-034274.

References

[1] S. Fatikow, J. Seyfried, S. Fahlbusch, A. Buerkle, and F. Schmoeckel, "A flexible microrobot-based microassembly station," *Journal of Intelligent and Robotic Systems*, no. 27, pp. 135–169, 2000.

[2] F. Schmoeckel and S. Fatikow, "Smart flexible microrobots for sem applications," in *SPIE's 7th Int. Symp. on Smart Structures and Materials: Integrated Systems*, 2000.

[3] S. Martel, A. Saraswat, and I. Hunter, "Fundamentals of piezoceramic actuation for micrometer and sub-micrometer motions for the nanowalker robot," in *SPIE2000*, 2000.

[4] S. Martel and I. Hunter, "Nanofactories based on a fleet of scientific instruments configured as miniature autonomous robots," *Jornal of Micromechatronics*, vol. 2, no. 3-4, pp. 201–214, 2004.

[5] W. Driesen, T. Varidel, S. Regnier, and J.-M. Breguet, "Micro manipulation by adhesion with two collaborating mobile micro robots," *Journal of Micromechatronics and Microengineering*, vol. 15, pp. 259–267, 2005.

[6] A.Bergander, W. Driesen, A. Lal, T. Varidel, M. Meizoso, H. Bleule, and J.-M. Breguet, "Position feedback for microrobots based on scanning probe microscopy," *Proceedings of 2004 IEEE/RSJ International Conference on Intelligent Robots and Systems*, September 2004.

[7] H. Aoyama, "Precise miniature robots and desktop flexible production," *Proc. of International Workshop on Microfactories, Japan*, pp. 145–156, 1998.

[8] H. Aoyama and A. Hayashi, "Multiple micro robots for desktop precise production," *Proc. of 1st International Conference of European Society for Precision Engineering and Nanotechnology*, vol. 1, pp. 60–63, 1999.

[9] S. Fatikow, *Mikrorobotik und Mikrosystemtechnik*. University of Oldenburg, Lecture notes, 2004, vol. 5.

[10] H. Hülsen, "Self-organising locally interpolating maps in control engineering," Ph.D. dissertation, University of Oldenburg, Germany, March 2007.

[11] A. Kortschack and S. Fatikow, "Development of a mobile nanohandling robot," *Journal of Micromechatronics*, pp. 249–269, 2004.

[12] A. Kortschack, A. Shirinov, T. Trüper, and S. Fatikow, "Development of mobile versatile nanohandling microrobots: design, driving principles, haptic control," *Robotica*, vol. 23, no. 4, pp. 419–434, 2005.

[13] S. Fahlbusch, S. Fatikow, S. Garnica, H. Huelsen, and A. Kortschack, "Development of a nanohandling robot cell," *Proc. of the 11th Mediterranean Conference on Control and Automation*, June 2003, t2-008.

[14] N. LaserPlussAG, *RayCutter 3200 manual*, LaserPluss AG, 2006.

[15] N.N., *Comsol Multiphysics Manual*, Comsol Multiphysics, 2007.